JAMECH
Vol. 45, No. 1, Sep. 2014, pp. 9-22

Nonlocal DQM for a Nonlinear Buckling Analysis of DLGSs Integrated with Zno Piezoelectric Layers

Ali Ghorbanpour Arani[1*], Abdolhossein Fereidoon[2], Reza Kolahchi[3]

1. Professor, Faculty of Mechanical Engineering, University of Kashan, Kashan, Iran

2. Professor, Department of Mechanical Engineering, Faculty of Engineering, University of Semnan, Semnan, Iran

3. Ph.D. Candidate, Faculty of Mechanical Engineering, University of Kashan, Kashan, Iran

Received 25 August 2014; Accepted 7 October 2014

Abstract

The nonlocal nonlinear buckling of a double layer graphene sheet (DLGS) covered by zinc oxide (ZnO) piezoelectric layers is investigated in this study. The surrounding circumstances of the system are considered as a Pasternak foundation including spring constants and a shear layer. Graphene sheets are subjected to longitudinal magnetic field and biaxial forces. On the other hand, the ZnO piezoelectric layer is subjected to an electric field. Eringen's nonlocal theory is used for considering small-scale effects. Classical plate theory (CPT) is employed to model the plates. Nonlinear Von-Karman theory, the energy method and Hamilton's principle are utilized to derive the size dependent governing equations. The known numerical differential quadrature method (DQM) is applied to obtain a nonlocal nonlinear buckling load. The detailed parametric study is conducted focusing on the effects of magnetic field strength, the dimensions of plates, small-scale effects and the intensity of the stiffness matrix on the nonlocal nonlinear buckling load of system. Results indicate that intensifying magnetic field makes the system more stable. Furthermore, increase in thickness of both piezoelectric and graphene layers makes the system stiffer, and consequently the buckling load becomes larger. The results of this study might be useful for the designing and manufacturing of graphene-based structures in micro or nanoelectromechanical systems.

Keywords: *DLGS, DQM, nonlinear buckling, ZnO piezoelectric layer.*

1. Introduction

Graphene sheets are one of the most famous and beloved types of carbon structures among researchers. The study of the mechanical behaviour of graphene sheets under different types of boundary conditions and subjected to various kinds of loading configurations has been receiving considerable interest from many researchers. This is because of their valuable properties. The primary and most popular definition of a single-layer graphene sheet (SLGS) accepted by the scientific communities is presented as: a flat monolayer of carbon atoms tightly packed into a two dimensional honeycomb lattice in which carbon atoms bond

* Corresponding Author. Tel.: +98 3155912450
Email: aghorban@kashanu.ac.ir

covalently with their neighbours [1]. Graphene sheets (GS) have extraordinary properties of physical, chemical and electrical types. Here are some of these properties which are mentioned in references [2-4]: strong mechanical strength (Young's modulus=1.0 TPa), large thermal conductivity (thermal conductivity=3000 W/km), excellent electric conductivity (electric conductivity up to 6000 S/cm), high surface area and unusual optical properties. Because of these stupendous and heralded properties, GSs can be used in many nanostructures such as nanosensors, nanooptomechanical systems, super capacitors, nanocomposites and so on [5,6].

The mechanical aspects of GSs and nanoplates have been investigated in the papers available in the literature. Pradhan and Kumar [7] studied the vibration of GSs using nonlocal elasticity and the DQM approach. They have investigated the effects of parameters such as graphene dimensions, nonlocal parameters, material properties and different boundary conditions on the dimensionless frequency of an orthotropic SLGS. Pradhan and Murmu [8] explored the small-scale effect on the buckling analysis of a SLGS resting on an elastic medium based on nonlocal plate theory. The results of their study show that the buckling load of GS depends strongly on the small-scale effects and stiffness of the elastic foundation. The thermal buckling properties of a nanoplate with small-scale effects were studied by Wang et al. [9] based on the nonlocal continuum theory. From this work, it can be observed that the small-scale effects are significant for the thermal buckling properties. Pradhan and Phadikar [10] investigated the small-scale effects on the vibration of multi-layer graphene sheets (MLGSs) using nonlocal continuum mechanics. Narendar and [11] investigated buckling analysis of orthotropic nanoplates such as graphene using the two-variable refined plate theory and nonlocal small-scale effects. It has been proven that the nondimensional buckling load of the orthotropic nanoplate is always smaller than that of the isotropic nanoplate. Liew et al. [12] explored nanovibration of GSs resting on an elastic medium. The presence of Van der walls (Vdw) force between graphene layers influences their natural frequency. GSs react to applied magnetic fields. This problem was considered by Murmu et al. [13] in their study. Based on their results, applying an in-plane magnetic field to SLGS enhances its natural frequency. Mohammadi et al. [14] analysed the transverse free vibration of circular GSs under different boundary conditions using nonlocal continuum mechanics. In an investigation, Ghorbanpour Arani et al. [15] presented a buckling analysis and smart control of SLGS using polyvinylidene fluoride (PVDF) based on nonlocal Mindlin plate theory. Furthermore, Ghorbanpour Arani et al. [16] investigated the elastic foundation effect on the nonlinear thermal vibration of an orthotropic DLGS.

On the other hand, creating composite or hybrid structures to achieve new materials with modified properties has a particular importance. By doing so, desirable properties are at hand. At the macro-scale, Hosseini Hashemi et al. [17] worked on finding an exact solution for the vibration of thick circular plates made of functionally graded material (FGM) covered by piezoelectric layers. In their study, the plates have been modelled using third order plate theory. Furthermore, the same author, in another study [18] examined a three dimensional Ritz solution for the free vibrations of annular plates made of FGM covered by piezoelectric layers. At the nano-scale, a buckling analysis of a carbon nanotube (CNT) as a core covered by ZnO layer subjected to both electrical field and mechanical strain was done by Zhang et al. [19]. Jiang and Gao [20] in an investigation proposed the fabrication and characterization of ZnO-coated multi-walled carbon nanotubes with enhanced photocatalytic activity. Huang et al. [21] explored a stable super hydrophobic surface using CNTs coated with a ZnO thin film.

The use of graphene-based structures has received considerable attention due to their thaumaturgic properties. The design and manufacture of stable systems are of common concern to researchers. Thus, using the results of this study, the buckling of the system can be postponed by changing parameters such as magnetic field intensity, length of plates and, particularly, the thickness of the ZnO layer. With a literature search, it can be found that there is no paper which conducts a buckling analysis of a DLGS covered by ZnO layers. Motivated by these considerations, in order to optimize the design of nanostructures, our aim is to investigate the stability control of DLGS

based on CPT. Herein, DLGS is covered by a ZnO piezoelectric layer, surrounded by a Pasternak medium, and subjected to both magnetic and electric fields. The influence of small-scale parameters, the elastic medium, the length of the plates and the magnetic field intensity on the buckling behaviour of DLGS have been taken into account.

2. A review of nonlocal theory

According to nonlocal piezoelasticity theory, the stress and electric displacement filed of a particular point depend not only on strain and electric filed components at the same point but also on all other points of the body. This statement of nonlocal theory can be formulated as nonlocal constitutive behaviour as follows [22,23].

$$\begin{aligned}\left(1-\mu\nabla^2\right)\sigma_{ij}^{nl} &= \sigma_{ij}^{l}\\ \left(1-\mu\nabla^2\right)D_{ij}^{nl} &= D_{ij}^{l}\end{aligned} \tag{1}$$

where σ_{ij}^{nl} and σ_{ij}^{l} are nonlocal stress tensor and local stress tensors, respectively. D_{ij}^{nl} and D_{ij}^{nl} denote components of nonlocal and local electric displacement, respectively. $\mu=(e_0a)^2$ represents the small-scale effect on the response of structures at nanosize and ∇^2 is the Laplacian operator.

3. Modelling of the problem

3.1. Geometrical description of the problem

A schematic configuration of the problem has been illustrated in Figure 1. As can be seen in Figure 1, a double layer graphene sheet is covered by two ZnO piezoelectric layers. The thicknesses of the graphene and piezoelectric layer are distinct, and are denoted by h_g and h_p, respectively. The interaction between graphene layers is modelled by Vdw force. The whole system is surrounded by a Pasternak foundation. Magnetic and electric fields are applied to the graphene and piezoelectric layers, respectively. Furthermore, a biaxial force is applied to the graphene sheets. Before continuing, it must be noted that the system shown in Figure 1 is divided into two systems. System 1 is considered as the upper piezoelectric and graphene layers, and system 2 is considered as the lower ones.

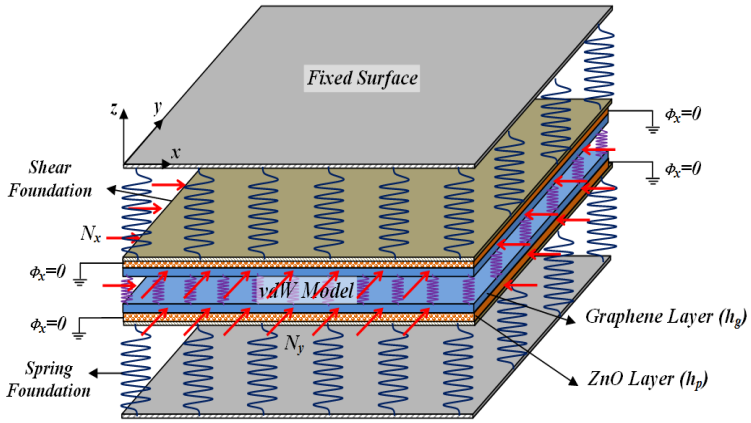

Fig. 1a. Schematic of double-layer graphene sheet covered by ZnO piezoelectric layer

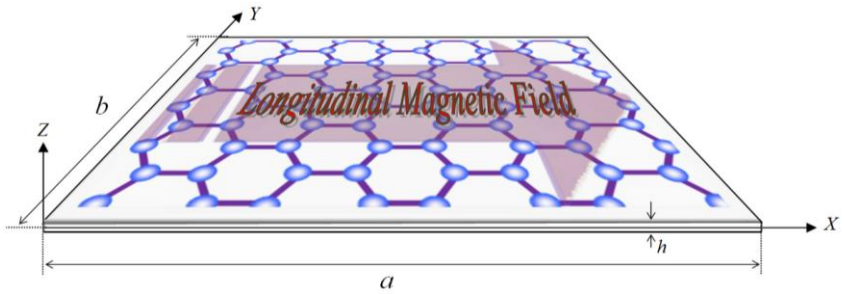

Fig. 1b. Direction of applied magnetic field to graphene sheets

3.2. Governing equations of motion

In this section, the aim is to obtain governing equations of motion by means of Hamilton's principle. In this study, all the layers have been simulated by CPT. The displacement field for CPT is presented as [24]:

$$\begin{aligned} u(x,y,z,t) &= u_0(x,y,t) - z\,\frac{\partial w_0}{\partial x} \\ v(x,y,z,t) &= v_0(x,y,t) - z\,\frac{\partial w_0}{\partial y} \\ w(x,y,z,t) &= w_0(x,y,t) \end{aligned} \tag{2}$$

where (u_0, v_0, w_0) is an arbitrary point on the middle surface of the plate. The nonlinear von-Karman strains are given by [24]:

$$\begin{pmatrix} \varepsilon_{xx} \\ \varepsilon_{yy} \\ \gamma_{xy} \end{pmatrix} = \begin{pmatrix} \varepsilon^0_{xx} \\ \varepsilon^0_{yy} \\ \gamma^0_{xy} \end{pmatrix} + z \begin{pmatrix} \varepsilon^1_{xx} \\ \varepsilon^1_{yy} \\ \gamma^1_{xy} \end{pmatrix} \tag{3}$$

where

$$\left(\varepsilon^0\right) = \begin{pmatrix} \varepsilon^0_{xx} \\ \varepsilon^0_{yy} \\ \gamma^0_{xy} \end{pmatrix} = \begin{pmatrix} \dfrac{\partial u_0}{\partial x} + \dfrac{1}{2}\left(\dfrac{\partial w_0}{\partial x}\right)^2 \\ \dfrac{\partial v_0}{\partial y} + \dfrac{1}{2}\left(\dfrac{\partial w_0}{\partial y}\right)^2 \\ \dfrac{\partial u_0}{\partial y} + \dfrac{\partial v_0}{\partial x} + \dfrac{\partial w_0}{\partial x}\dfrac{\partial w_0}{\partial y} \end{pmatrix},$$

$$\left(\varepsilon^1\right) = \begin{pmatrix} \varepsilon^1_{xx} \\ \varepsilon^1_{yy} \\ \gamma^1_{xy} \end{pmatrix} = \begin{pmatrix} -\dfrac{\partial^2 w_0}{\partial x^2} \\ -\dfrac{\partial^2 w_0}{\partial y^2} \\ -2\dfrac{\partial^2 w_0}{\partial x \partial y} \end{pmatrix}. \tag{4}$$

Constitutive equations for ZnO material can be defined as follows [25].

$$\begin{bmatrix} \sigma^P_{xx} \\ \sigma^P_{yy} \\ \sigma^P_{zz} \\ \sigma^P_{yz} \\ \sigma^P_{zx} \\ \sigma^P_{xy} \end{bmatrix} = \begin{bmatrix} C_{11} & C_{12} & C_{13} & 0 & 0 & 0 \\ C_{12} & C_{11} & C_{13} & 0 & 0 & 0 \\ C_{13} & C_{13} & C_{33} & 0 & 0 & 0 \\ 0 & 0 & 0 & C_{44} & 0 & 0 \\ 0 & 0 & 0 & 0 & C_{44} & 0 \\ 0 & 0 & 0 & 0 & 0 & \dfrac{C_{11}-C_{12}}{2} \end{bmatrix} \begin{bmatrix} \varepsilon_{xx} \\ \varepsilon_{yy} \\ \varepsilon_{zz} \\ \gamma_{yz} \\ \gamma_{zx} \\ \gamma_{xy} \end{bmatrix} - \begin{bmatrix} e_{31} & 0 & 0 \\ e_{31} & 0 & 0 \\ e_{33} & 0 & 0 \\ 0 & e_{15} & 0 \\ 0 & 0 & e_{15} \\ 0 & 0 & 0 \end{bmatrix} \begin{bmatrix} E_x \\ E_y \\ E_z \end{bmatrix} \tag{5}$$

where C_{11}, C_{12}, C_{13}, C_{33}, C_{44} are linear elastic constants and e_{31}, e_{33}, e_{15} are linear piezoelectric constants. Superscript P refers to the piezoelectric material. E_i $(i=x,y,z)$ shows electric filed intensity and can be obtained from [26].

$$E_i = -\frac{\partial \varphi}{\partial i} \quad i = x, y, z \tag{6}$$

where ϕ is the electric potential applied to the piezoelectric layers. On the other hand, the electric displacement of this particular material is presented as [25]:

$$\begin{bmatrix} D_{xx} \\ D_{yy} \\ D_{zz} \end{bmatrix} = \begin{bmatrix} e_{31} & e_{31} & e_{33} & 0 & 0 & 0 \\ 0 & 0 & 0 & e_{15} & 0 & 0 \\ 0 & 0 & 0 & 0 & e_{15} & 0 \end{bmatrix} \begin{bmatrix} \varepsilon_{xx} \\ \varepsilon_{yy} \\ \varepsilon_{zz} \\ \gamma_{yz} \\ \gamma_{zx} \\ \gamma_{xy} \end{bmatrix} + \begin{bmatrix} K_{11} & 0 & 0 \\ 0 & K_{11} & 0 \\ 0 & 0 & K_{33} \end{bmatrix} \begin{bmatrix} E_x \\ E_y \\ E_z \end{bmatrix} \tag{7}$$

In this equation, K_{11}, K_{33} are dielectric constants. In this investigation, electric field is applied along x direction and along two other directions considered zero. For our particular problem, constitutive and electric displacement equations are summarized as follows.

$$\begin{aligned} \sigma^P_{xx} &= C_{11}\varepsilon_{xx} + C_{12}\varepsilon_{yy} - e_{31}E_x \\ \sigma^P_{yy} &= C_{12}\varepsilon_{xx} + C_{11}\varepsilon_{yy} - e_{31}E_x \\ \sigma^P_{xy} &= \frac{C_{11}-C_{12}}{2}\gamma_{xy} \\ D_{xx} &= e_{31}\varepsilon_{xx} + e_{31}\varepsilon_{yy} + K_{11}E_x \end{aligned} \tag{8}$$

On the other hand, constitutive equations for orthotropic graphene sheets modelled by CPT are [24]:

$$\begin{bmatrix} \sigma^G_{xx} \\ \sigma^G_{yy} \\ \sigma^G_{xy} \end{bmatrix} = \begin{bmatrix} Q_{11} & Q_{12} & 0 \\ Q_{12} & Q_{22} & 0 \\ 0 & 0 & Q_{66} \end{bmatrix} \begin{bmatrix} \varepsilon_{xx} \\ \varepsilon_{yy} \\ \gamma_{xy} \end{bmatrix} \tag{9}$$

where Q_{ij} $(i,j = 1,2,6)$ are the stress-reduced plane and their values can be obtained using the following formulae.

$$
\begin{aligned}
Q_{11} &= \frac{E_1}{1-\nu_{12}\nu_{21}} \\
Q_{12} &= \frac{\nu_{12}E_2}{1-\nu_{12}\nu_{21}} = \frac{\nu_{21}E_1}{1-\nu_{12}\nu_{21}} \\
Q_{22} &= \frac{E_2}{1-\nu_{12}\nu_{21}} \\
Q_{66} &= G_{12}
\end{aligned}
\tag{10}
$$

where E_1 and E_2 are elastic modulus along 1 and 2 directions, respectively. ν_{12} and ν_{21} are Poisson constants. G_{12} is a shear modulus. As mentioned earlier, the governing equations are obtained using Hamilton's principle. Hamilton's principle in its familiar form is expressed as:

$$
\int_0^T \left(\delta U_{tot} + \delta V_{tot}\right) dt = 0 \tag{11}
$$

in which U_{tot} and V_{tot} are the total potential energy and work done by external forces, respectively.

3.2.1. Virtual potential energy and virtual external works

Virtual potential energy and virtual work done by external forces of both graphene and piezoelectric layers have been calculated separately and are added together at the end.

The virtual potential energy and virtual work for the piezoelectric layer are:

$$
\begin{aligned}
\delta U_P &= \int_S \int_0^{h_p} \begin{pmatrix} \overset{P}{\sigma}_{xx}\delta\varepsilon_{xx} + \overset{P}{\sigma}_{yy}\delta\varepsilon_{yy} \\ +\overset{P}{\sigma}_{xy}\delta\gamma_{xy} - D_{xx}\,\delta E_x \end{pmatrix} dz\,dx\,dy = \\
&\int_S \Big\{ \int_0^{h_p} \Big[\overset{P}{\sigma}_{xx}\left(\delta\overset{0}{\varepsilon}_{xx} + z\,\delta\overset{1}{\varepsilon}_{xx}\right) \\
&+\overset{P}{\sigma}_{yy}\left(\delta\overset{0}{\varepsilon}_{yy} + z\,\delta\overset{1}{\varepsilon}_{yy}\right) + \overset{P}{\sigma}_{xy}\left(\delta\overset{0}{\gamma}_{xy} + z\,\delta\overset{1}{\gamma}_{xy}\right) \\
&- D_{xx}\,\delta E_x \Big] dz \Big\} dx\,dy
\end{aligned}
\tag{12}
$$

$$
\delta V_P = -\int_S \left[\; q_P(x,y)\,\delta w \;\right] dx\,dy \tag{13}
$$

in which subscript p refers to the piezoelectric and q_p are all the transverse forces acting on the piezoelectric layer. Because of the Pasternak foundation, transverse forces are:

$$
q_P(x,y) = -K_w w_1 + G_P \nabla^2 w_1 \tag{14}
$$

In the above equation, K_w and G_P are the Winkler and shear layer of the Pasternak foundation coefficients, respectively.

Similarly, the virtual potential energy and virtual work due to external forces for graphene are as follows.

$$
\begin{aligned}
\delta U_G &= \int_S \int_{-h_g}^0 \left(\sigma_{xx}^G \delta\varepsilon_{xx} + \sigma_{yy}^G \delta\varepsilon_{yy} + \sigma_{xy}^G \delta\gamma_{xy}\right) dz\,dx\,dy \\
&= \int_S \Big\{ \int_{-h_g}^0 \Big[\sigma_{xx}^G \left(\delta\varepsilon_{xx}^0 + z\,\delta\varepsilon_{xx}^1\right) + \sigma_{yy}^G \left(\delta\varepsilon_{yy}^0 + z\,\delta\varepsilon_{yy}^1\right) \\
&+ \sigma_{xy}^G \left(\delta\gamma_{xy}^0 + z\,\delta\gamma_{xy}^1\right) \Big] dz \Big\} dx\,dy
\end{aligned}
\tag{15}
$$

$$
\delta V_G = -\int_S \begin{pmatrix} \int_{-h_g}^0 \left(f_{mz}\delta w + f_{my}\delta v\right) dz \\ -C_v(w_1 - w_2)\delta w \end{pmatrix} dx dy \tag{16}
$$

Subscript G denotes parameters corresponding to graphene. In this equation, f_{mz} and f_{my} are Lorentz forces along the z and y axes, respectively. They can be calculated as [26]:

$$
\begin{aligned}
f_{mx} &= 0 \\
f_{my} &= \eta H_x^2 \left(\frac{\partial^2 v}{\partial x^2} + \frac{\partial^2 v}{\partial y^2} + \frac{\partial^2 w}{\partial y\,\partial z} \right) \\
f_{mz} &= \eta H_x^2 \left(\frac{\partial^2 w}{\partial x^2} + \frac{\partial^2 w}{\partial y^2} + \frac{\partial^2 v}{\partial y\,\partial z} \right)
\end{aligned}
\tag{17}
$$

Since displacement components are independent of the thickness of the plate, the final form of the Lorentz force used in this investigation is:

$$
f = \left(0, \eta H_x^2 \left(\frac{\partial^2 v}{\partial x^2} + \frac{\partial^2 v}{\partial y^2}\right), \eta H_x^2 \left(\frac{\partial^2 w}{\partial x^2} + \frac{\partial^2 w}{\partial y^2}\right)\right). \tag{18}
$$

Using the internal integral of Eq. (16) and by Eq. (17), their values along the thickness can be obtained.

$$
q_{mz} = \int_{-h_g}^0 f_{mz}\,dz = \eta\, h_g\, H_x^2 \left(\frac{\partial^2 w}{\partial x^2} + \frac{\partial^2 w}{\partial y^2} \right) \tag{19}
$$

$$
q_{my} = \int_{-h_g}^0 f_{my}\,dz = \eta\, h_g\, H_x^2 \left(\frac{\partial^2 v}{\partial x^2} + \frac{\partial^2 v}{\partial y^2} \right) \tag{20}
$$

The total virtual potential and virtual work of the external forces for system 1 are:

$$\delta U_{tot} = \delta U_G + \delta U_P = \int_S \Big\{ \int \Big[\Big(\sigma^G_{xx} + \sigma^P_{xx} \Big) \Big(\delta \varepsilon^0_{xx} + z\, \delta \varepsilon^1_{xx} \Big) + \Big(\sigma^G_{yy} + \sigma^P_{yy} \Big) \Big(\delta \varepsilon^0_{yy} + z\, \delta \varepsilon^1_{yy} \Big) + \Big(\sigma^G_{xy} + \sigma^P_{xy} \Big) \Big(\delta \gamma^0_{xy} + z\, \delta \gamma^1_{xy} \Big) - D_{xx}\, \delta E_x \Big] dz \Big\} dx\, dy \tag{21}$$

Substituting Equations. (13), (16) and (21) into Equation (11) and integrating them, the following time integration is obtained.

$$0 = \int_0^T \Big\{ \int_S \Big[N_{xx}\, \delta \varepsilon^0_{xx} + M_{xx}\, \delta \varepsilon^1_{xx} + N_{yy}\, \delta \varepsilon^0_{yy} + M_{yy}\, \delta \varepsilon^1_{yy} + N_{xy}\, \delta \gamma^0_{xy} + M_{xy}\, \delta \gamma^1_{xy} - q_P\, \delta w - q_{mz}\, \delta w - q_{my}\, \delta v + C_v (w_1 - w_2) - G\, \delta E_x \Big] \delta w \; dx\, dy \Big\} dt \tag{22}$$

Considering the above equation, the following equations are defined.

$$\begin{aligned} N_{xx} &= N^G_{xx} + N^P_{xx} \;, N_{yy} = N^G_{yy} + N^P_{yy} \\ N_{xy} &= N^G_{xy} + N^P_{xy}, M_{xx} = M^G_{xx} + M^P_{xx} \\ M_{yy} &= M^G_{yy} + M^P_{yy} \;, M_{xy} = M^G_{xy} + M^P_{xy} \end{aligned} \tag{23}$$

where in this equation, the stress and moment resultants are calculated as:

$$\begin{Bmatrix} \boldsymbol{N}^G_{xx} \\ \boldsymbol{N}^G_{yy} \\ \boldsymbol{N}^G_{xy} \end{Bmatrix} = \int_{-h_g}^{0} \begin{Bmatrix} \boldsymbol{\sigma}_{xx} \\ \boldsymbol{\sigma}_{yy} \\ \boldsymbol{\sigma}_{xy} \end{Bmatrix} \boldsymbol{dz}$$

$$\begin{Bmatrix} \boldsymbol{M}_{xx} \\ \boldsymbol{M}_{yy} \\ \boldsymbol{M}_{xy} \end{Bmatrix} = \int_{-h_g}^{0} \begin{Bmatrix} \boldsymbol{\sigma}_{xx} \\ \boldsymbol{\sigma}_{yy} \\ \boldsymbol{\sigma}_{xy} \end{Bmatrix} \boldsymbol{z}\; \boldsymbol{dz}$$

$$\begin{Bmatrix} \boldsymbol{N}^P_{xx} \\ \boldsymbol{N}^P_{yy} \\ \boldsymbol{N}^P_{xy} \end{Bmatrix} = \int_{0}^{h_P} \begin{Bmatrix} \boldsymbol{\sigma}_{xx} \\ \boldsymbol{\sigma}_{yy} \\ \boldsymbol{\sigma}_{xy} \end{Bmatrix} \boldsymbol{dz} \tag{24}$$

$$\begin{Bmatrix} \boldsymbol{M}_{xx} \\ \boldsymbol{M}_{yy} \\ \boldsymbol{M}_{xy} \end{Bmatrix} = \int_{0}^{h_P} \begin{Bmatrix} \boldsymbol{\sigma}_{xx} \\ \boldsymbol{\sigma}_{yy} \\ \boldsymbol{\sigma}_{xy} \end{Bmatrix} \boldsymbol{z}\; \boldsymbol{dz}$$

$$\boldsymbol{G} = \int_{0}^{h_P} \boldsymbol{D}_{xx}\, \boldsymbol{dz}$$

Considering Equation (22) and using integration by parts, the results after the separation of the coefficients of the same variables has the local form of equations of motion in terms of displacement, in which nonlocal Eringen theory has yet not been applied to them. To this end, using this theory, the nonlocal form of Equations (22) after the separation of the same variables for system 1 are as follows:

δu_1:

$$A'_{11}\left(\frac{\partial^2 u_1}{\partial x^2} + \frac{\partial^2 w_1}{\partial x^2}\frac{\partial w_1}{\partial x}\right) + A'_{12}\left(\frac{\partial^2 v_1}{\partial y\, \partial x} + \frac{\partial^2 w_1}{\partial y\, \partial x}\frac{\partial w_1}{\partial y}\right) + A'_{66}\left(\frac{\partial^2 u_1}{\partial y^2} + \frac{\partial^2 v_1}{\partial x\, \partial y} + \frac{\partial^2 w_1}{\partial x\, \partial y}\frac{\partial w_1}{\partial y} + \frac{\partial^2 w_1}{\partial y^2}\frac{\partial w_1}{\partial x}\right) - B'_{11}\frac{\partial^3 w_1}{\partial x^3} - B'_{12}\frac{\partial^3 w_1}{\partial x\, \partial y^2} - 2B'_{66}\frac{\partial^3 w_1}{\partial x\, \partial y^2} + n_{31}\frac{\partial^2 \phi_1}{\partial x^2} = 0 \tag{25a}$$

δv_1:

$$A'_{12}\left(\frac{\partial^2 u_1}{\partial x\, \partial y} + \frac{\partial^2 w_1}{\partial x\, \partial y}\frac{\partial w_1}{\partial x}\right) + A'_{22}\left(\frac{\partial^2 v_1}{\partial y^2} + \frac{\partial^2 w_1}{\partial y^2}\frac{\partial w_1}{\partial y}\right) + A'_{66}\left(\frac{\partial^2 u_1}{\partial y\, \partial x} + \frac{\partial^2 v_1}{\partial x^2} + \frac{\partial^2 w_1}{\partial x\, \partial y}\frac{\partial w_1}{\partial x} + \frac{\partial^2 w_1}{\partial x^2}\frac{\partial w_1}{\partial y}\right) + \eta\, hg\, H_x^2\left(\frac{\partial^2 v_1}{\partial x^2} + \frac{\partial^2 v_1}{\partial y^2}\right) - B'_{12}\frac{\partial^3 w_1}{\partial x^2 \partial y} - 2B'_{66}\frac{\partial^3 w_1}{\partial x^2 \partial y} - B'_{22}\frac{\partial^3 w_1}{\partial y^3} + n_{31}\frac{\partial^2 \phi_1}{\partial x^2} - \mu\left[\eta\, hg\, H_x^2\left(\frac{\partial^4 v_1}{\partial x^4} + 2\frac{\partial^4 v_1}{\partial x^2 \partial y^2} + \frac{\partial^4 v_1}{\partial y^4}\right)\right] = 0 \tag{25b}$$

δw_1:

$$
\begin{aligned}
&-D'_{11}\frac{\partial^4 w_1}{\partial x^4}-2D'_{12}\frac{\partial^4 w_1}{\partial y^2\partial x^2}-D'_{22}\frac{\partial^4 w_1}{\partial y^4}+A'_{11}\left(\frac{\partial u_1}{\partial x}\frac{\partial^2 w_1}{\partial x^2}+\frac{1}{2}\left(\frac{\partial w_1}{\partial x}\right)^2\frac{\partial^2 w_1}{\partial x^2}\right)+A'_{12}\left(\frac{\partial v_1}{\partial y}\frac{\partial^2 w_1}{\partial x^2}+\frac{1}{2}\left(\frac{\partial w_1}{\partial y}\right)^2\frac{\partial^2 w_1}{\partial x^2}\right)-n_{31}\frac{\partial \phi_1}{\partial x}\frac{\partial^2 w_1}{\partial x^2}\\
&+2A'_{66}\left(\frac{\partial u_1}{\partial y}\frac{\partial^2 w_1}{\partial y\partial x}+\frac{\partial v_1}{\partial x}\frac{\partial^2 w_1}{\partial y\partial x}+\frac{\partial w_1}{\partial x}\frac{\partial w_1}{\partial y}\frac{\partial^2 w_1}{\partial y\partial x}\right)+A'_{12}\left(\frac{\partial u_1}{\partial x}\frac{\partial^2 w_1}{\partial y^2}+\frac{1}{2}\left(\frac{\partial w_1}{\partial x}\right)^2\frac{\partial^2 w_1}{\partial y^2}\right)+A'_{22}\left(\frac{\partial v_1}{\partial y}\frac{\partial^2 w_1}{\partial y^2}+\frac{1}{2}\left(\frac{\partial w_1}{\partial y}\right)^2\frac{\partial^2 w_1}{\partial y^2}\right)\\
&+n_{31}\frac{\partial \phi_1}{\partial x}\frac{\partial^2 w_1}{\partial y^2}-K_w w_1+G_p\left(\frac{\partial^2 w_1}{\partial x^2}+\frac{\partial^2 w_1}{\partial y^2}\right)+N_0\frac{\partial^2 w_1}{\partial x^2}+\alpha N_0\frac{\partial^2 w_1}{\partial y^2}-\eta hg H_x^2\left(\frac{\partial^2 v_1}{\partial x^2}\frac{\partial w_1}{\partial y}+\frac{\partial^2 v_1}{\partial y^2}\frac{\partial w_1}{\partial y}\right)\\
&+\eta hg H_x^2\left(\frac{\partial^2 w_1}{\partial x^2}+\frac{\partial^2 w_1}{\partial y^2}\right)-C_v\left(w_1-w_2\right)B'_{11}\left(\frac{\partial^3 u_1}{\partial x^3}+\frac{\partial^2 w_1}{\partial x^2}\frac{\partial^2 w_1}{\partial x^2}+\frac{\partial w_1}{\partial x}\frac{\partial^3 w_1}{\partial x^3}\right)+B'_{12}\left(\frac{\partial^3 v_1}{\partial x^2\partial y}+\frac{\partial^2 w_1}{\partial x\partial y}\frac{\partial^2 w_1}{\partial x\partial y}+\frac{\partial w_1}{\partial y}\frac{\partial^3 w_1}{\partial x^2\partial y}\right)\\
&+2B'_{66}\left(\frac{\partial^3 u_1}{\partial x\partial y^2}+\frac{\partial^3 v_1}{\partial x^2\partial y}+\frac{\partial^3 w_1}{\partial x^2\partial y}\frac{\partial w_1}{\partial y}+\frac{\partial^2 w_1}{\partial x\partial y}\frac{\partial^2 w_1}{\partial x\partial y}+\frac{\partial^2 w_1}{\partial x^2}\frac{\partial^2 w_1}{\partial y^2}+\frac{\partial w_1}{\partial x}\frac{\partial^3 w_1}{\partial x\partial y^2}\right)-4D'_{66}\frac{\partial^4 w_1}{\partial x^2\partial y^2}\\
&+B'_{12}\left(\frac{\partial^3 u_1}{\partial x\partial y^2}+\frac{\partial^2 w_1}{\partial x\partial y}\frac{\partial^2 w_1}{\partial x\partial y}+\frac{\partial w_1}{\partial x}\frac{\partial^3 w_1}{\partial x\partial y^2}\right)+B'_{22}\left(\frac{\partial^3 v_1}{\partial y^3}+\frac{\partial^2 w_1}{\partial y^2}\frac{\partial^2 w_1}{\partial y^2}+\frac{\partial w_1}{\partial y}\frac{\partial^3 w_1}{\partial y^3}\right)-B'_{11}\frac{\partial^2 w_1}{\partial x^2}\frac{\partial^2 w_1}{\partial x^2}-2B'_{12}\frac{\partial^2 w_1}{\partial y^2}\frac{\partial^2 w_1}{\partial x^2}\\
&-4B'_{66}\frac{\partial^2 w_1}{\partial y\partial x}\frac{\partial^2 w_1}{\partial y\partial x}-B'_{22}\frac{\partial^2 w_1}{\partial y^2}\frac{\partial^2 w_1}{\partial y^2}+m_{311}\frac{\partial^3 \phi_1}{\partial x^3}+m_{311}\frac{\partial^3 \phi_1}{\partial x\partial y^2}-\mu\left[-K_w\left(\frac{\partial^2 w_1}{\partial x^2}+\frac{\partial^2 w_1}{\partial y^2}\right)-C_v\left(\frac{\partial^2 w_1}{\partial x^2}+\frac{\partial^2 w_1}{\partial y^2}-\frac{\partial^2 w_2}{\partial x^2}-\frac{\partial^2 w_2}{\partial y^2}\right)\right.\\
&+G_p\left(\frac{\partial^4 w_1}{\partial x^4}+2\frac{\partial^4 w_1}{\partial y^2\partial x^2}+\frac{\partial^4 w_1}{\partial y^4}\right)+\eta hg H_x^2\left(\frac{\partial^4 w_1}{\partial x^4}+2\frac{\partial^4 w_1}{\partial y^2\partial x^2}+\frac{\partial^4 w_1}{\partial y^4}\right)+\eta hg H_x^2\left[\frac{\partial^2 v_1}{\partial x^2}\frac{\partial^3 w_1}{\partial y\partial x^2}+\frac{\partial^2 v_1}{\partial y^2}\frac{\partial^3 w_1}{\partial y\partial x^2}+\frac{\partial^4 v_1}{\partial x^4}\frac{\partial w_1}{\partial y}+\frac{\partial^4 v_1}{\partial x^2\partial y^2}\frac{\partial w_1}{\partial y}\right.\\
&\left.\left.+\frac{\partial^2 v_1}{\partial x^2}\frac{\partial^3 w_1}{\partial y^3}+\frac{\partial^2 v_1}{\partial y^2}\frac{\partial^3 w_1}{\partial y^3}\frac{\partial^4 v_1}{\partial y^2\partial x^2}\frac{\partial w_1}{\partial y}+\frac{\partial^4 v_1}{\partial y^4}\frac{\partial w_1}{\partial y}+2\left(\frac{\partial^3 v_1}{\partial x^3}\frac{\partial^2 w_1}{\partial y\partial x}+\frac{\partial^3 v_1}{\partial y^2\partial x}\frac{\partial^2 w_1}{\partial y\partial x}+\frac{\partial^3 v_1}{\partial y\partial x^2}\frac{\partial^3 w_1}{\partial y^2}+\frac{\partial^3 v_1}{\partial y^3}\frac{\partial^2 w_1}{\partial y^2}\right)\right]\right]=0
\end{aligned}
\tag{25c}
$$

$\delta \phi_1$:

$$
n_{31}\left(\frac{\partial u_1}{\partial x}+\frac{1}{2}\left(\frac{\partial w_1}{\partial x}\right)^2+\frac{\partial v_1}{\partial y}+\frac{1}{2}\left(\frac{\partial w_1}{\partial y}\right)^2\right)-K_{11}hp\frac{\partial \phi_1}{\partial x}=0 \tag{25d}
$$

In the above equations, the following definitions have been utilized.

$$
\begin{aligned}
&A'_{11}=A_{11}^G+A_{11}^P, A'_{12}=A_{12}^G+A_{12}^P \quad , \quad A_{22}=A_{22}^G+A_{11}^P, A'_{66}=A_{66}^G+A_{66}^P\\
&B'_{11}=B_{11}^G+B_{11}^P, B'_{12}=B_{12}^G+B_{12}^P \quad , \quad B'_{22}=B_{22}^G+B_{11}^P, B'_{66}=B_{66}^G+B_{66}^P\\
&D'_{11}=D_{11}^P+D_{11}^G, D'_{12}=D_{12}^G+D_{12}^P \quad , \quad D'_{22}=D_{22}^G+D_{11}^P, D'_{66}=D_{66}^G+D_{66}^P
\end{aligned}
\tag{26}
$$

The coefficients corresponding to the piezoelectric layer are:

$$
\begin{aligned}
&\left(A_{11}^P, A_{12}^P, A_{66}^P\right)=\int_0^{h_p}\left(C_{11}, C_{12}, C_{66}\right)dz=\left(C_{11}, C_{12}, C_{66}\right)h_p\\
&\left(B_{11}^P, B_{12}^P, B_{66}^P\right)=\int_0^{h_p}\left(C_{11}, C_{12}, C_{66}\right)z\,dz=\frac{\left(C_{11},, C_{12}, C_{66}\right)}{2}{h_p}^2\\
&\left(D_{11}^P, D_{12}^P, D_{66}^P\right)=\int_0^{h_p}\left(C_{11}, C_{12}, C_{66}\right)z^2\,dz=\frac{\left(C_{11},, C_{12}, C_{66}\right)}{3}{h_p}^3\\
&n_{31}=\int_0^{h_p}e_{31}dz=e_{31}h_p,\ m_{311}=\int_0^{h_p}e_{31}z\,dz=\frac{e_{31}}{2}\left({h_p}^2\right)
\end{aligned}
\tag{27}
$$

where

$$
C_{66}=\frac{1}{2}\left(C_{11}-C_{12}\right) \tag{28}
$$

and the coefficients corresponding to the graphene layer are:

$$\left(A_{11}^{G},A_{12}^{G},A_{22}^{G},A_{66}^{G}\right)=\int_{-h_g}^{0}(Q_{11},Q_{12},Q_{22},Q_{66})dz=(Q_{11},Q_{12},Q_{22},Q_{66})h_g$$
$$\left(B_{11}^{G},B_{12}^{G},B_{22}^{G},B_{66}^{G}\right)=\int_{-h_g}^{0}(Q_{11},Q_{12},Q_{22},Q_{66})zdz=\frac{(Q_{11},Q_{12},Q_{22},Q_{66})}{2}\left(-{h_g}^{2}\right) \quad (29)$$
$$\left(D_{11}^{G},D_{12}^{G},D_{22}^{G},D_{66}^{G}\right)=\int_{-h_g}^{0}(Q_{11},Q_{12},Q_{22},Q_{66})z^{2}dz=\frac{(Q_{11},Q_{12},Q_{22},Q_{66})}{3}\left({h_g}^{3}\right)$$

In order to generalize the results of this investigation to any system consistent with our work, we have to utilize the dimensionless nonlocal form of Equations (25a-d). To this end, dimensionless parameters have been introduced as:

$$(\bar{u},\bar{v},\bar{w})=\frac{(u,v,w)}{h_g},\xi=\frac{x}{a},\theta=\frac{y}{b},\gamma=\frac{h_g}{a},\beta=\frac{h_g}{b},\bar{\phi}=\frac{\phi e_{31}}{C_{11}h_p}$$
$$en=\frac{e_0 a}{a},A_{12}''=\frac{A_{12}'}{A_{11}'},A_{66}''=\frac{A_{66}'}{A_{11}'},A_{22}''=\frac{A_{22}'}{A_{11}'},\tilde{A}_{66}=\frac{A_{66}'{h_g}^{2}}{D_{11}'}$$
$$n_{31}''=\frac{C_{11}h_p}{A_{11}'},\tilde{K}_w=\frac{K_w h_g a^{3}}{D_{11}'},\tilde{G}_p=\frac{G_p a h_g}{D_{11}'},\tilde{N}_0=\frac{N_0 a h_g}{D_{11}'}$$
$$\tilde{A}_{11}=\frac{A_{11}'{h_g}^{2}}{D_{11}'}\tilde{A}_{12}=\frac{A_{12}'{h_g}^{2}}{D_{11}'},\tilde{n}_{31}=\frac{C_{11}{h_g}^{3}}{D_{11}'},MP'=\frac{\eta H_x^{2}b}{A_{11}'} \quad (30)$$
$$MP''=\frac{\eta H_x^{2}{h_g}^{2}a}{D_{11}'},D_{22}''=\frac{D_{12}'}{D_{11}'},D_{12}''=\frac{D_{12}'}{D_{11}'},,D_{66}''=\frac{D_{66}'}{D_{11}'},\bar{K}_{11}=\frac{K_{11}C_{11}}{e_{31}^{2}}$$
$$B_{11}''=\frac{B_{11}}{A_{11}a},B_{12}''=\frac{B_{12}}{A_{11}a},B_{22}''=\frac{B_{22}}{A_{11}a},B_{66}''=\frac{B_{66}}{B_{11}a},\tilde{B}_{11}=\frac{B_{11}h_g}{D_{11}},\tilde{B}_{12}=\frac{B_{12}h_g}{D_{11}}$$
$$\tilde{B}_{22}=\frac{B_{22}h_g}{D_{11}},\tilde{m}_{311}=\frac{m_{311}C_{11}h_p}{e_{31}D_{11}},m_{311}'=\frac{m_{311}}{e_{31}a^{2}}$$
$$m_{311}=\frac{e_{31}}{2}hp^{2},f=\frac{h_p}{h_g}$$

Then, using these dimensionless parameters, Equations (25a-d) will change into the following form:

δu_i :

$$\gamma\left(\frac{\partial^2\bar{u}_i}{\partial\xi^2}+\gamma\frac{\partial^2\bar{w}_i}{\partial\xi^2}\frac{\partial\bar{w}_i}{\partial\xi}\right)+A_{12}''\beta\left(\frac{\partial^2\bar{v}_i}{\partial\theta\partial\xi}+\beta\frac{\partial^2\bar{w}_i}{\partial\theta\partial\xi}\frac{\partial\bar{w}_i}{\partial\theta}\right)+A_{66}''\beta\left(\frac{\beta}{\gamma}\frac{\partial^2\bar{u}_i}{\partial\theta^2}+\frac{\partial^2\bar{v}_i}{\partial\theta\partial\xi}+\beta\frac{\partial^2\bar{w}_i}{\partial\theta\partial\xi}\frac{\partial\bar{w}_i}{\partial\theta}+\beta\frac{\partial^2\bar{w}_i}{\partial\theta^2}\frac{\partial\bar{w}_i}{\partial\xi}\right) \quad (31a)$$
$$+n_{31}''\gamma f\frac{\partial^2\bar{\phi}_i}{\partial\xi^2}-B_{11}''\gamma\frac{\partial^3\bar{w}_i}{\partial\xi^3}-B_{12}''\frac{\beta^2}{\gamma}\frac{\partial^3\bar{w}_i}{\partial\xi\partial\theta^2}-2B_{66}''\frac{\beta^2}{\gamma}\frac{\partial^3\bar{w}_i}{\partial\xi\partial\theta^2}=0,$$

δv_i :

$$A_{12}''\gamma\left(\frac{\partial^2\bar{u}_i}{\partial\xi\partial\theta}+\gamma\frac{\partial^2\bar{w}_i}{\partial\xi\partial\theta}\frac{\partial\bar{w}_i}{\partial\xi}\right)+A_{22}''\beta\left(\frac{\partial^2\bar{v}_i}{\partial\theta^2}+\beta\frac{\partial^2\bar{w}_i}{\partial\theta^2}\frac{\partial\bar{w}_i}{\partial\theta}\right)+A_{66}''\gamma\left(\frac{\partial^2\bar{u}_i}{\partial\theta\partial\xi}+\frac{\gamma}{\beta}\frac{\partial^2\bar{v}_i}{\partial\xi^2}+\gamma\frac{\partial^2\bar{w}_i}{\partial\theta\partial\xi}\frac{\partial\bar{w}_i}{\partial\xi}+\gamma\frac{\partial^2\bar{w}_i}{\partial\xi^2}\frac{\partial\bar{w}_i}{\partial\theta}\right)$$
$$+MP'\left(\frac{\gamma^2}{\beta}\frac{\partial^2\bar{v}_i}{\partial\xi^2}+\beta\frac{\partial^2\bar{v}_i}{\partial\theta^2}\right)-B_{12}''\gamma\frac{\partial^3\bar{w}_i}{\partial\xi^2\partial\theta}-B_{22}''\frac{\beta^2}{\gamma}\frac{\partial^3\bar{w}_i}{\partial\theta^3}-2B_{66}''\gamma\frac{\partial^3\bar{w}_i}{\partial\xi^2\partial\theta}+n_{31}''f\gamma\frac{\partial^2\bar{\phi}_i}{\partial\xi\partial\theta} \quad (31b)$$
$$-(en)^2MP'\left[\gamma^2\frac{\partial^4\bar{v}_i}{\partial\xi^4}+2\beta^2\frac{\partial^4\bar{v}_i}{\partial\xi^2\partial\theta^2}+\left(\frac{\beta}{\gamma}\right)^2\beta^2\frac{\partial^4\bar{v}_i}{\partial\theta^4}\right]=0,$$

δw_i :

$$
\begin{aligned}
&-\gamma\frac{\partial^4\bar{w}_i}{\partial\xi^4}-2D''_{12}\frac{\beta^2}{\gamma}\frac{\partial^4\bar{w}_i}{\partial\theta^2\partial\xi^2}-D''_{22}\frac{\beta^4}{\gamma^3}\frac{\partial^4\bar{w}_i}{\partial\theta^4}+\tilde{A}_{11}\left(\frac{\partial\bar{u}_i}{\partial\xi}\frac{\partial^2\bar{w}_i}{\partial\xi^2}+\frac{\gamma}{2}\left(\frac{\partial\bar{w}_i}{\partial\xi}\right)^2\frac{\partial^2\bar{w}_i}{\partial\xi^2}\right)\\
&+\tilde{A}_{12}\left(\frac{\beta}{\gamma}\frac{\partial\bar{v}_i}{\partial\theta}\frac{\partial^2\bar{w}_i}{\partial\xi^2}+\frac{\beta^2}{2\gamma}\left(\frac{\partial\bar{w}_i}{\partial\theta}\right)^2\frac{\partial^2\bar{w}_i}{\partial\xi^2}\right)+\tilde{n}_{31}\frac{\partial\bar{\phi}_i}{\partial\xi}\frac{\partial^2\bar{w}_i}{\partial\xi^2}+\tilde{n}_{31}\left(\frac{\beta}{\gamma}\right)^2\frac{\partial\bar{\phi}_i}{\partial\xi}\frac{\partial^2\bar{w}_i}{\partial\theta^2}\\
&+2\tilde{A}_{66}\frac{\beta}{\gamma}\left(\frac{\beta}{\gamma}\frac{\partial\bar{u}_i}{\partial\theta}\frac{\partial^2\bar{w}_i}{\partial\theta\partial\xi}+\frac{\partial\bar{v}_i}{\partial\xi}\frac{\partial^2\bar{w}_i}{\partial\theta\partial\xi}+\beta\frac{\partial\bar{w}_i}{\partial\xi}\frac{\partial\bar{w}_i}{\partial\theta}\frac{\partial^2\bar{w}_i}{\partial\theta\partial\xi}\right)+\tilde{A}_{12}\frac{\beta}{\gamma}\left(\frac{\beta}{\gamma}\frac{\partial\bar{u}_i}{\partial\xi}\frac{\partial^2\bar{w}_i}{\partial\theta^2}+\frac{\beta}{2}\left(\frac{\partial\bar{w}_i}{\partial\xi}\right)^2\frac{\partial^2\bar{w}_i}{\partial\theta^2}\right)\\
&+\tilde{A}_{22}\left(\frac{\beta}{\gamma}\right)^3\left(\frac{\partial\bar{v}_i}{\partial\theta}\frac{\partial^2\bar{w}_i}{\partial\theta^2}+\frac{\beta}{2}\left(\frac{\partial\bar{w}_i}{\partial\theta}\right)^2\frac{\partial^2\bar{w}_i}{\partial\theta^2}\right)+\tilde{B}_{11}\left(\frac{\partial^3\bar{u}_i}{\partial\xi^3}+\gamma\frac{\partial^2\bar{w}_i}{\partial\xi^2}\frac{\partial^2\bar{w}_i}{\partial\xi^2}+\gamma\frac{\partial\bar{w}_i}{\partial\xi}\frac{\partial^3\bar{w}_i}{\partial\xi^3}\right)\\
&\tilde{B}_{12}\left(\frac{\beta}{\gamma}\frac{\partial^3\bar{v}_i}{\partial\xi^2\partial\theta}+\frac{\beta^2}{\gamma}\frac{\partial^2\bar{w}_i}{\partial\theta\partial\xi}\frac{\partial^2\bar{w}_i}{\partial\theta\partial\xi}+\frac{\beta^2}{\gamma}\frac{\partial\bar{w}_i}{\partial\theta}\frac{\partial^3\bar{w}_i}{\partial\xi^2\partial\theta}\right)\\
&+2\tilde{B}_{66}\left(\left(\frac{\beta}{\gamma}\right)^2\frac{\partial^3\bar{u}_i}{\partial\xi\partial\theta^2}+\frac{\beta}{\gamma}\frac{\partial^3\bar{v}_i}{\partial\xi^2\partial\theta}+\frac{\beta^2}{\gamma}\frac{\partial\bar{w}_i}{\partial\theta}\frac{\partial^3\bar{w}_i}{\partial\xi^2\partial\theta}+\frac{\beta^2}{\gamma}\frac{\partial^2\bar{w}_i}{\partial\theta\partial\xi}\frac{\partial^2\bar{w}_i}{\partial\theta\partial\xi}+\frac{\beta^2}{\gamma}\frac{\partial^2\bar{w}_i}{\partial\xi^2}\frac{\partial^2\bar{w}_i}{\partial\theta^2}+\frac{\beta^2}{\gamma}\frac{\partial\bar{w}_i}{\partial\xi}\frac{\partial^3\bar{w}_i}{\partial\theta^2\partial\xi}\right)\\
&-4D''_{66}\frac{\beta^2}{\gamma}\frac{\partial^4\bar{w}_i}{\partial\theta^2\partial\xi^2}+\tilde{B}_{12}\left(\left(\frac{\beta}{\gamma}\right)^2\frac{\partial^3\bar{u}_i}{\partial\theta^2\partial\xi}+\frac{\beta^2}{\gamma}\frac{\partial^2\bar{w}_i}{\partial\theta\partial\xi}\frac{\partial^2\bar{w}_i}{\partial\theta\partial\xi}+\frac{\beta^2}{\gamma}\frac{\partial\bar{w}_i}{\partial\xi}\frac{\partial^3\bar{w}_i}{\partial\theta^2\partial\xi}\right)\\
&-\tilde{B}_{11}\gamma\frac{\partial^2\bar{w}_i}{\partial\xi^2}\frac{\partial^2\bar{w}_i}{\partial\xi^2}-\tilde{B}_{12}\frac{\beta^2}{\gamma}\frac{\partial^2\bar{w}_i}{\partial\xi^2}\frac{\partial^2\bar{w}_i}{\partial\theta^2}-4\tilde{B}_{66}\frac{\beta^2}{\gamma}\frac{\partial^2\bar{w}_i}{\partial\theta\partial\xi}\frac{\partial^2\bar{w}_i}{\partial\theta\partial\xi}-\tilde{B}_{12}\frac{\beta^2}{\gamma}\frac{\partial^2\bar{w}_i}{\partial\xi^2}\frac{\partial^2\bar{w}_i}{\partial\theta^2}\\
&-\tilde{B}_{22}\frac{\beta^4}{\gamma^3}\frac{\partial^2\bar{w}_i}{\partial\theta^2}\frac{\partial^2\bar{w}_i}{\partial\theta^2}-\tilde{K}_w\bar{w}_i+\tilde{G}_p\left(\frac{\partial^2\bar{w}_i}{\partial\xi^2}+\left(\frac{\beta}{\gamma}\right)^2\frac{\partial^2\bar{w}_i}{\partial\theta^2}\right)+\tilde{N}_0\frac{\partial^2\bar{w}_i}{\partial\xi^2}+\alpha\tilde{N}_0\left(\frac{\beta}{\gamma}\right)^2\frac{\partial^2\bar{w}_i}{\partial\theta^2}\\
&-MP''\left(\beta\frac{\partial^2\bar{v}_i}{\partial\xi^2}\frac{\partial\bar{w}_i}{\partial\theta}+\beta\left(\frac{\beta}{\gamma}\right)^2\frac{\partial^2\bar{v}_i}{\partial\theta^2}\frac{\partial\bar{w}_i}{\partial\theta}-\frac{\partial^2\bar{w}_i}{\partial\xi^2}-\left(\frac{\beta}{\gamma}\right)^2\frac{\partial^2\bar{w}_i}{\partial\theta^2}\right)\\
&-\chi\tilde{C}_V\left(\bar{w}_1-\bar{w}_2\right)+(en)^2\left[-\tilde{K}_w\left(\frac{\partial^2\bar{w}_i}{\partial\xi^2}+\left(\frac{\beta}{\gamma}\right)^2\frac{\partial^2\bar{w}_i}{\partial\theta^2}\right)+\tilde{G}_p\left(\frac{\partial^4\bar{w}_i}{\partial\xi^4}+2\left(\frac{\beta}{\gamma}\right)^2\frac{\partial^4\bar{w}_i}{\partial\xi^2\partial\theta^2}+\left(\frac{\beta}{\gamma}\right)^4\frac{\partial^4\bar{w}_i}{\partial\theta^4}\right)+\right.\\
&MP''\left[\frac{\partial^2\bar{v}_i}{\partial\xi^2}\frac{\partial^3\bar{w}_i}{\partial\theta\partial\xi^2}+\left(\frac{\beta}{\gamma}\right)^2\frac{\partial^2\bar{v}_i}{\partial\theta^2}\frac{\partial^3\bar{w}_i}{\partial\theta\partial\xi^2}+\frac{\partial^4\bar{v}_i}{\partial\xi^4}\frac{\partial\bar{w}_i}{\partial\theta}+\left(\frac{\beta}{\gamma}\right)^2\frac{\partial^4\bar{v}_i}{\partial\theta^2\partial\xi^2}\frac{\partial\bar{w}_i}{\partial\theta}\right.\\
&+\left(\frac{\beta}{\gamma}\right)^2\frac{\partial^2\bar{v}_i}{\partial\xi^2}\frac{\partial^3\bar{w}_i}{\partial\theta^3}+\left(\frac{\beta}{\gamma}\right)^4\frac{\partial^2\bar{v}_i}{\partial\theta^2}\frac{\partial^3\bar{w}_i}{\partial\theta^3}+\frac{\partial^4\bar{w}_i}{\partial\xi^4}+\left(\frac{\beta}{\gamma}\right)^2\frac{\partial^4\bar{v}_i}{\partial\theta^2\partial\xi^2}\frac{\partial\bar{w}_i}{\partial\theta}\\
&\left.\left.+\left(\frac{\beta}{\gamma}\right)^4\frac{\partial^4\bar{v}_i}{\partial\theta^4}\frac{\partial\bar{w}_i}{\partial\theta}+2\left(\frac{\partial^3\bar{v}_i}{\partial\xi^3}\frac{\partial^2\bar{w}_i}{\partial\theta\partial\xi}+\frac{\partial^3\bar{v}_i}{\partial\theta^2\partial\xi}\frac{\partial^2\bar{w}_i}{\partial\theta\partial\xi}+\frac{\partial^3\bar{v}_i}{\partial\theta\partial\xi^2}\frac{\partial^2\bar{w}_i}{\partial\theta^2}+\frac{\partial^3\bar{v}_i}{\partial\theta^3}\frac{\partial^2\bar{w}_i}{\partial\theta^2}\right)\right]\right.\\
&\left.+\left(\frac{\beta}{\gamma}\right)^4\frac{\partial^4\bar{w}_i}{\partial\theta^4}+2\left(\frac{\beta}{\gamma}\right)2\frac{\partial^4\bar{w}_i}{\partial\xi^2\partial\theta^2}\right]+\chi\tilde{C}_V\left(\frac{\partial^2\bar{w}_1}{\partial\xi^2}+\frac{\partial^2\bar{w}_1}{\partial\theta^2}-\frac{\partial^2\bar{w}_2}{\partial\xi^2}-\frac{\partial^2\bar{w}_2}{\partial\theta^2}\right)\Bigg]=0
\end{aligned}
\tag{31c}
$$

$\delta\phi_i$:

$$
\gamma\frac{\partial\bar{u}_i}{\partial\xi}+\frac{\gamma^2}{2}\left(\frac{\partial\bar{w}_i}{\partial\xi}\right)^2+\beta\frac{\partial\bar{v}_i}{\partial\theta}+\frac{\beta^2}{2}\left(\frac{\partial\bar{w}_i}{\partial\theta}\right)^2-\gamma\bar{K}_{11}f\,\gamma\frac{\partial\bar{\phi}_i}{\partial\xi}-\frac{m'_{311}}{f}\frac{\partial^2\bar{w}_i}{\partial\xi^2}-\frac{m'_{311}}{f}\left(\frac{\beta}{\gamma}\right)^2\frac{\partial^2\bar{w}_i}{\partial\theta^2}=0 \tag{31d}
$$

in which index i can adopt 1 and 2 for system 1 and 2, respectively. X is +1 for system 1 and is -1 for system 2.

4. Solution procedure

Because of nonlinear nature of the equations, the closed-form solution is out of scope, and then we must explore the solution to the problem using numerical methods. One of the most famous and applicable methods is DQM. In this method equations will be discretized and will be rearranged in a matrix form.

4.1. An introduction to DQ method

For two dimensional problems, the partial differential is approximated as [28]:

$$\begin{aligned}
&\frac{\partial^n f\left(x_i,y_j\right)}{\partial x^n}=\sum_{k=1}^{N_x}A_{x,ik}f\left(x_k,y_j\right),\ n=1,...,N_x-1\\
&\frac{\partial^m f\left(x_i,y_j\right)}{\partial y^m}=\sum_{k=1}^{N_y}A_{y,jk}f\left(x_i,y_k\right),m=1,...,N_y-1\\
&\frac{\partial^{n+m} f\left(x_i,y_j\right)}{\partial x^n}=\sum_{k=1}^{N_x}A_{x,ik}f\left(x_k,y_j\right)
\end{aligned}\tag{32}$$

in which $f(x,y)$ is a function of two variables, N_x and N_y are a number of points along x and y directions, respectively, $A_{x,ik}$ is the weighting coefficient. The meshing of plates was done using the Chebyshev distribution formula. Weighting coefficients are calculated as [28]:

$$\begin{aligned}
A_{ij}^{(1)}&=\begin{cases}\dfrac{M\left(x_i\right)}{\left(x_i-x_j\right)M\left(x_j\right)} & i\neq j,\ \ i,j=1,2,...,N_x\\ -\sum\limits_{j=1,j\neq i}^{N_x}A_{ij}^{(1)} & i=j,\ \ i,j=1,2,...,N_x\end{cases}\\
B_{ij}^{(1)}&=\begin{cases}\dfrac{P\left(y_i\right)}{\left(y_i-y_j\right)P\left(y_j\right)} & i\neq j,\ \ i,j=1,2,...,N_y\\ -\sum\limits_{j=1,j\neq i}^{N_y}A_{ij}^{(1)} & i=j,\ \ i,j=1,2,...,N_y\end{cases}
\end{aligned}\tag{33}$$

where

$$\begin{aligned}
M\left(x_i\right)&=\prod_{j=1,j\neq i}^{N_x}\left(x_i-x_j\right)\\
P\left(y_i\right)&=\prod_{j=1,j\neq i}^{N_y}\left(y_i-y_j\right)
\end{aligned}\tag{34}$$

For a higher order of derivatives, we have employed the following formula:

$$\begin{aligned}
\left[A^{(n)}\right]&=\left[A^{(1)}\right]^n\\
\left[B^{(m)}\right]&=\left[B^{(1)}\right]^m
\end{aligned}\tag{35}$$

In this study, we have considered boundary conditions for all the edges of plates as simply supported. These boundary conditions can be expressed as:

$$\begin{aligned}
&u=v=w=0 \quad @ \quad x=0,a \ \ \& \ \ y=0,b\\
&\frac{\partial^2 w}{\partial x^2}=0 \quad @ \quad x=0,a\\
&\frac{\partial^2 w}{\partial y^2}=0 \quad @ \quad y=0,b
\end{aligned}\tag{36}$$

4.2. Buckling analysis of the problem

Applying the DQ method to all the governing equations of motion and boundary conditions including system 1 and 2, the following eigenvalue problem can be obtained.

$$\left(\left[K_L+K_{NL}\right]+\bar{N}_0\left[K_g\right]\right)\{d\}=0\tag{37}$$

In which $[K_L]$ and $[K_{NL}]$ are linear and nonlinear portions of stiffness matrix. $[K_g]$ also is a force coefficient matrix. $\bar{N}_0$ expresses the critical buckling load and $\{d\}$ denotes the displacement matrix and is defined as:

$$\{d\}=\left\{\{\bar{u}\}^T,\{\bar{v}\}^T,\{\bar{w}\}^T,\{\bar{\varphi}\}^T\right\}.\tag{38}$$

The eigenvalue problem (Equation 37) must be solved using an iteration process until a convergence criterion satisfied. At first, the nonlinear portion of the stiffness matrix is ignored, the eigenvalue problem is solved, and the eigenvalues and eigenvectors of Equation (37) are obtained. These eigenvectors are used to achieve eigenvectors of a nonlinear problem. This process iterates until the following convergence criterion is satisfied.

$$\frac{\alpha_{i-1}-\alpha_i}{\alpha_{i-1}}<0.01\%.\tag{39}$$

in which α is an eigenvector corresponding to a linear eigenvalue problem.

5. Numerical results and discussion

The nonlinear instability of double layer graphene sheets covered by piezoelectric layers and subjected to biaxial forces, magnetic and electric

fields and surrounded by a Pasternak foundation, is investigated in this paper. In the following figures, the effects of the parameters such as stiffness of circumstance, magnetic intensity, nonlocal-scale number, thicknesses of graphene and piezoelectric layer, and Vander walls on the instability of the system are investigated. The properties of graphene and ZnO piezoelectric material are presented in Table 1 [25].

Table 1. Material properties of ZnO and DLGS.

ZnO	DLGS
$c_{11} = 207\,(GPa)$	$E_1 = 1765\,(GPa)$
$c_{12} = 117.7\,(GPa)$	$E_2 = 1588\,(GPa)$
$e_{31} = -0.51$	$\nu_{12} = \nu_{21} = 0.3$
$k_{11} = 7.77\,e(-11)$	

In all the figures presented in this section, the vertical axis denotes the buckling load and the horizontal axis denotes small-scale parameters.

At first, we investigated the effect of the nonlinearity of equations on the instability of the system. Figure 2 shows the effects of considering and omitting nonlinearity terms in equations on the instability of the system. As can be seen from Figure 2, omitting nonlinear terms results in a decrease in the stability of the system. In other words, designing based on a linear state is to some extent conservative. With an increase in nonlocal parameters, two diagrams tend to converge.

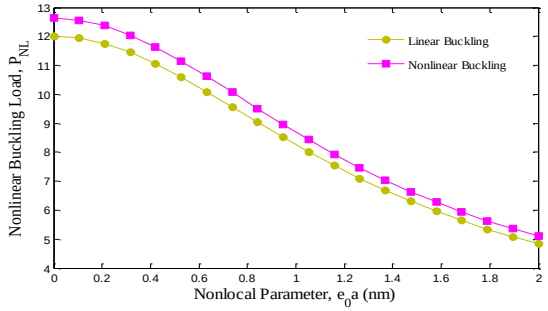

Fig. 2. A comparison for stability between linear and nonlinear state

In order to explore the effects of the different types of surrounding circumstances, Figure 3 has been plotted. As can be expected, without an elastic medium, the load required for the system to fail in the buckling shape is the least. With appending springs and developing a Winkler foundation, the stability of the system increased considerably. On the other hand, a Pasternak foundation makes the system stiffer, and then the stability of system will be the most sensitive. By increasing nonlocal parameters, the difference between the diagrams will be the same.

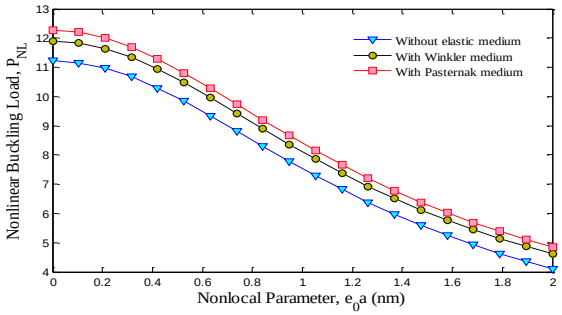

Fig. 3. Influence of different types of surrounding circumstances

Figure 4 depicts the effects of changing the length of the plates on the load required for buckling. Obviously, with an increase in dimensions of the plate, the instability of the system decreases. This behaviour of the system is expected as we know that there is an inverse relation between buckling load and the length of plate. Another point that can be comprehended from this figure is that for smaller plates, e.g., a=10 or 20 nm, the effects of nonlocal parameters are more obvious. The reason is that, as can be interpreted from the name of small-scale parameters, it is a criterion for the measurement of the exiguity of a system, then for larger systems its effect becomes less than for smaller ones.

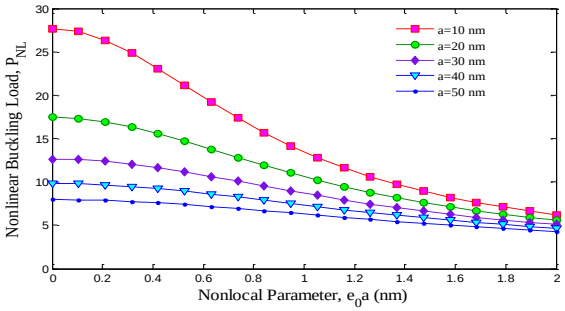

Fig. 4. Nonlinear buckling load versus nonlocal parameter for various lengths of plates

The influence of the thickness of graphene and piezoelectric layers on the stability of the systems is shown in Figure 5a and b, respectively. Clearly, an increase in the thickness of both piezoelectric and graphene layers makes the system stiffer, and consequently the buckling

load becomes larger. This is because from our primary knowledge of the strength of materials that the relation between buckling load and stiffness of a system is direct. The only difference is that, at the end of the spectrum of nonlocal parameters, the diagrams corresponding to the graphene layer are going to converge.

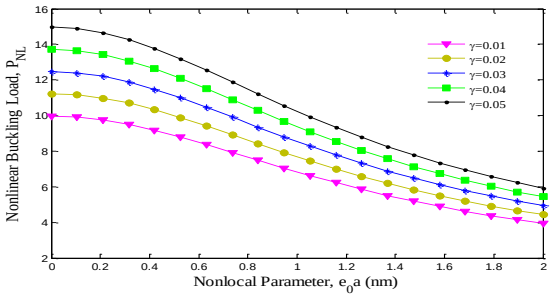

Fig. 5a. Effect of graphene thickness on stability of the system

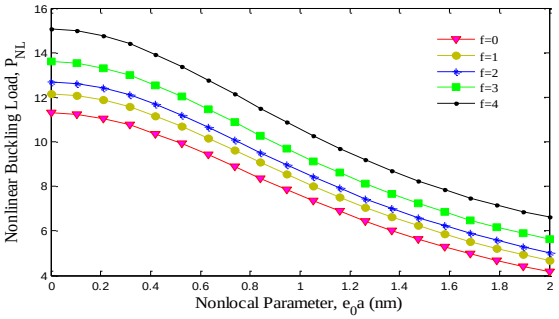

Fig. 5b. Effect of piezoelectric thickness on stability of the system

One of the most important parameters that can be changed to control the stability of a system is magnetic field intensity. To this end, Figure 6 was drawn. It is understood from this figure that increasing magnetic field intensity has a positive influence on the stability of the system. An increase in the small-scale has little effect on the difference between diagrams.

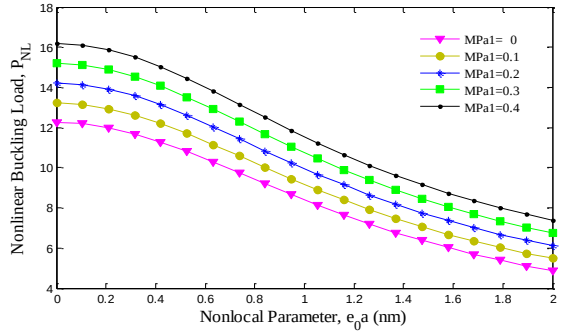

Fig. 6. Variation of nonlinear buckling load against nonlocal parameter with magnetic field intensity

To explore the effect due to the presence of Vander walls force, Figure 7 was plotted. This figure illustrates that, because of presence of Vander walls force, the system becomes stiffer in comparison to an absence of it, and the result is a more stable system than expected. Another conclusion that can be seen is that the influence of an increase in nonlocal parameters on the difference between the two diagrams is slight and can be ignored.

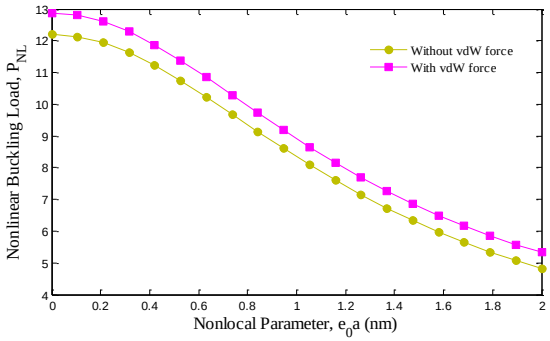

Fig. 7. Effect of presence and absence of Vander walls force on stability of system

Figure 8 presents a variation of the buckling load of the system with various values of spring coefficients corresponding to the Pasternak foundation. As illustrated in this figure, with an increase in the stiffness of the springs, the load required to buckle the system increases perceptibly.

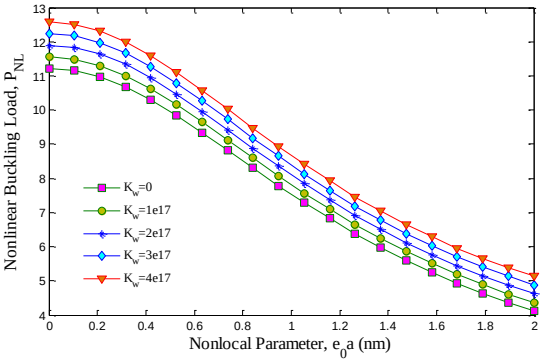

Fig. 8. Variation of stability of system versus small scale parameter for different values of stiffness

The final figure of this section is Figure 9 in which a comparison between two states is presented. In one diagram the graphene layers undergo only in-plane uniaxial forces while in the other they are subjected to in-plane biaxial forces. This figure shows that in a uniaxial state more powerful forces are needed to destabilize the system. The tendency of the two diagrams is

convergence at the end of the nonlocal parameter spectrum.

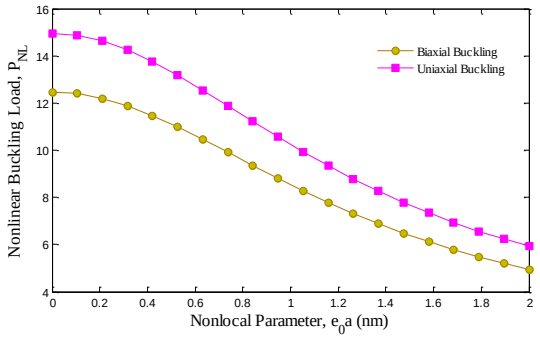

Fig. 9. A comparison for stability of the system between uniaxial and biaxial forces

6. Conclusion

In this paper, the nonlinear instability of a double layer graphene sheet covered by ZnO piezoelectric layers, subjected to biaxial forces, electric and magnetic fields, and surrounded by a Pasternak foundation was investigated. Using Figures 2-9, some major conclusions can be summarized as follows:

1. Omitting nonlinear terms from the equations results in a conservative analysis.
2. As the system becomes stiffer the load required to buckle it becomes larger.
3. Increasing the nonlocal parameter leads to a decrease in system stability.
4. There was an inverse relation between the dimensions of the plates and the stability of the system.
5. Intensifying the magnetic field makes the system more stable.
6. The presence of Vander walls force has a positive role on the stability of the system.

Acknowledgement

The authors are grateful to University of Kashan for supporting this work by Grant No. 363443/24**."**

References

[1].Yang M., Javadi A., Li H., Gong H.S., 2010, Ultrasensitive immunosensor for the detection of cancer biomarker based on graphene sheet, Biosens. Bioelectron. **26**: 560-565.

[2].Oh J.S., Hwang Ta., Nam G.Y., Hong J.P., Bae A.H., Son S.I., Lee G.H., Sung H.K., Choi H.R., Koo J.C., Nam J.D., 2012, Chemically-modified graphene sheets as an active layer for eco-friendly metal electroplating on plastic substrates, Thin Solid Film. **521**: 270-274.

[3].Chen C., Fu W., Yu C. A., 2012, facile one-step hydrothermal method to produce α-MnO2/graphene sheet composites and its electrochemical properties, Mater. Lett. **82**: 133-136.

[4].Baykasoglu C., Mugan A., 2012, Dynamic analysis of single-layer graphene sheets, Comput. Mater. Sci. **55**: 228-236.

[5].Qian Y., Wang C., Le Z.G., 2011, Decorating graphene sheets with Pt nanoparticles using sodium citrate as reductant, Appl. Surf. Sci. **257**: 10758-10759.

[6].Jomehzadeh E., Saidi A.R., 2011, A study on large amplitude vibration of multilayered graphene sheets, Comput. Mater. Sci. **50**: 1043-1051.

[7].Pradhan S.C., Kumar A., 2011, Vibration analysis of orthotropic graphene sheets using nonlocal elasticity theory and differential quadrature method, Compos. Struct. **93**: 774-779.

[8].Pradhan S.C., Murmu T., 2010, Small scale effect on the buckling analysis of single-layered graphene sheet embedded in an elastic medium based on nonlocal plate theory, Physica E **42**: 1293-1301.

[9].Wang Y.Z., Cui H.T., Li F.M., Kishimoto K., 2013, Thermal buckling of a nanoplate with small-scale effects, Acta Mech. **224**: 1299-1307.

[10]. Pradhan S.C., Phadikar J.K., 2009, Small scale effect on vibration of embedded multilayered graphene sheets based on nonlocal continuum models, Phys. Lett. A. **373**: 1062-1069.

[11]. Narendar S., Gopalakrishnan S., 2012, Scale effects on buckling analysis of orthotropic nanoplates based on nonlocal two-variable refined plate theory, Acta Mech. **223**: 395-413.

[12]. Liew K.M., He X.Q., Kitipornchai S., 2006, Predicting nanovibration of multi-layered graphene sheets embedded in an elastic matrix, Acta. Mater. **54**: 4229-4236.

[13]. Murmu T., McCarthy M.A., Adhikari S., 2013, In-plane magnetic field affected transverse vibration of embedded single-layer graphene sheets using equivalent nonlocal elasticity approach, Comp. Struct. **96**: 57-63.

[14]. Mohammadi M., Ghayour M., Farajpour A., 2013, Free transverse vibration analysis of

circular and annular graphene sheets with various boundary conditions using the nonlocal continuum plate model, Compos. Part B: Eng. **45**: 32-42.

[15]. Ghorbanpour Arani A., Kolahchi R., Vossough H., 2012, Buckling analysis and smart control of SLGS using elastically coupled PVDF nanoplate based on the nonlocal Mindlin plate theory, Physica B **407**: 4458-4465.

[16]. Ghorbanpour Arani A., Kolahchi R., Mosallaie Barzoki A.A., Mozdianfard M.R., Farahani S.M.N. 2012, Elastic foundation effect on nonlinear thermo-vibration of embedded double layered orthotropic graphene sheets using differential quadrature method, J. Mech. Eng. Sci. **227**: 1-18.

[17]. Hashemi Sh.H., Es'haghi M., Karimi M., 2010, Closed-form vibration analysis of thick annular functionally graded plates with integrated piezoelectric layers, Int. J. Mech. Sci. **52**: 410-428.

[18]. Hashemi Sh.H., Monfared M.A., Taher H.R.D., 2010, A 3-D Ritz solution for free vibration of circular/annular functionally graded plates integrated with piezoelectric layers, Int. J. Eng. Sci. **48**: 1971-1984.

[19]. Zhang J., Wang R., Wang C., 2012, Piezoelectric ZnO-CNT nanotubes under axial strain and electrical voltage, Physica E **46**: 105-112.

[20]. Jiang L.Q., Gao L., 2005, Fabrication and characterization of ZnO-coated multi-walled carbon nanotubes with enhanced photocatalytic activity, Mat. Chem. Phy. **91**: 313-316.

[21]. Huang L., Lau S.P., Yang H.Y., Leong E.S.P., Yu S.F., 2005, Stable Superhydrophobic Surface via Carbon Nanotubes Coated with a ZnO Thin Film, J. Phys. Chem. B **109**: 7746-7748.

[22]. Han J.H., Lee I., 1998, Analysis of composite plates with piezoelectric actuators for vibration control using layerwise displacement theory, Compos. Part B: Eng. **29**: 621-632.

[23]. Ke L.L., Wang Y.Sh., Wang Zh.D., 2012, Nonlinear vibration of the piezoelectric nanobeams based on the nonlocal theory, Compos. Struct. **96**: 2038-2042.

[24]. Reddy J.N., 2004, Mechanics of laminated composite plates and shells, theory and analysis. CRC Press, London.

[25]. Gao Y., Wang Z.L., 2007, Electrostatic Potential in a Bent Piezoelectric Nanowire. The Fundamental Theory of Nanogenerator and Nanopiezotronics, Nano Lett. **7**: 2499-2505.

[26]. Ghorbanpour Arani A., Kolahchi R., Mosallaie Barzoki A.A., 2011, Effect of material in-homogeneity on electro-thermo-mechanical behaviors of functionally graded piezoelectric rotating shaft, Appl. Math. Model. **35**: 2771-2789.

[27]. Wang H., Dong K., Men F., Yan Y.J., Wang X., 2010, Influences of longitudinal magnetic field on wave propagation in carbon nanotubes embedded in elastic matrix, Appl. Math. Model. **34**: 878-889.

[28]. Shu C., 1990, Differential Quadrature and Its Application in Engineering. Springer, USA.